RADIATIVE FORCING BY CO2 OBSERVED AT TOP OF ATMOSPHERE FROM 2002-2019

Christopher Rentsch[1,1]

[1]N/A

November 30, 2022

Abstract

Spectroscopic measurements at top-of-atmosphere are uniquely capable of attributing changes in Earth's outgoing infrared radiation field to specific greenhouse gasses. The Atmospheric Infrared Sounder (AIRS) placed in orbit in 2002 has spectroscopically resolved a portion of Earth's outgoing longwave radiation for 17 years. Concurrently, atmospheric CO2 rose from 373 to 410 ppm, or 28% of the total increase over pre-industrial levels. The IPCC Fifth Assessment Report predicted 0.508±0.102 Wm-$^{\mathbf{2}}$ additional radiative forcing from this CO2 increase. Here it is shown that global measurements under nighttime, cloud-clear conditions reveal 0.358±0.067 Wm-$^{\mathbf{2}}$ of CO2-induced radiative forcing, or 70% of IPCC model predictions.

RADIATIVE FORCING BY CO_2 OBSERVED AT TOP OF ATMOSPHERE FROM 2002-2019

C. P. Rentsch

Midland, MI, USA

Key Points:

- The Atmospheric Infrared Sounder (AIRS) offers the longest observational record among all current and previous satellite spectrophotometers.
- Seventeen years of global nighttime, cloud-clear spectral radiance measurements reveal 0.358±0.067 Wm^{-2} of CO_2-induced radiative forcing.
- Observed CO_2 forcing is 70% of the effective radiative forcing predicted by the IPCC 5^{th} Assessment Report.

Abstract

Spectroscopic measurements at top-of-atmosphere are uniquely capable of attributing changes in Earth's outgoing infrared radiation field to specific greenhouse gasses. The Atmospheric Infrared Sounder (AIRS) placed in orbit in 2002 has spectroscopically resolved a portion of Earth's outgoing longwave radiation for 17 years. Concurrently, atmospheric CO_2 rose from 373 to 410 ppm, or 28% of the total increase over pre-industrial levels. The IPCC Fifth Assessment Report predicted 0.508 ± 0.102 Wm^{-2} additional radiative forcing from this CO_2 increase. Here it is shown that global measurements under nighttime, cloud-clear conditions reveal 0.358 ± 0.067 Wm^{-2} of CO_2-induced radiative forcing, or 70% of IPCC model predictions.

Introduction

Increasing infrared absorption caused by rising CO_2 is the foundational physical mechanism underpinning the anthropogenic global warming hypothesis. Despite numerous studies on global temperature trends and rising greenhouse gas concentrations, very few investigations offer long term spectrophotometric measurement of CO_2 altering Earth's outgoing longwave radiation (OLR). Harries et al. (2001) compared 529 OLR spectra measured by the IRIS satellite in 1970 to 4,061 spectra measured by IMG in 1996 over the Pacific Ocean. Feldman et al. (2015) reported increasing downwelling longwave radiation (DLR) in two 1.6° conical upward views of the atmosphere between 2000 and 2010 (figure 1). Neither study provides a global assessment of CO_2-induced radiative forc-

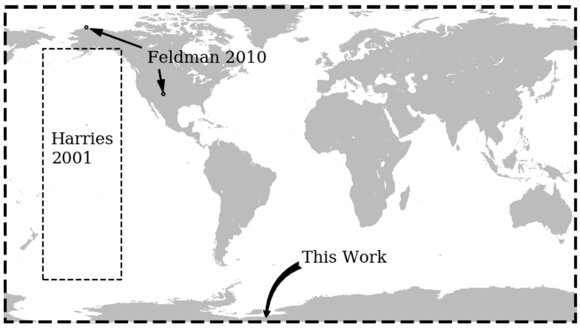

Figure 1. Measurement coverage for this work and select prior works by others

ing. The Atmospheric Infrared Spectrophotometer (AIRS) offers the longest record among all current or previous satellite spectrophotometers and has measured Earth's OLR while atmospheric CO_2 concentration rose from 373 to 410 ppm, 28% of the total increase since 1750. This work examines 50.7 billion global nighttime, cloud-clear spectral radiance measurements (hereafter: radiances) made by AIRS during the last seventeen years. Figure 2 exemplifies a single OLR spectrum comprised of 2,378 radiances. AIRS does not have measurement capability at <649.6 cm^{-1}, 1136-1217 cm^{-1} or 1614-2181 cm^{-1}.

1 Data

The majority of satellite views of Earth contain clouds that reflect or absorb upwelling infrared (IR). Cloud-clear scenes are preferred to avoid attributing cloud-induced OLR reductions to CO_2. The AIRS version 6 level 2 data product (Teixeira, 2013) quantifies fractional cloud content ($Tot\_Cld4\_CCfinal$ field in $AIRS2CCF$.006) ranging from 0.00 to 1.00. This work utilizes radiances with 0.00 cloud fraction; only 11% or radiances

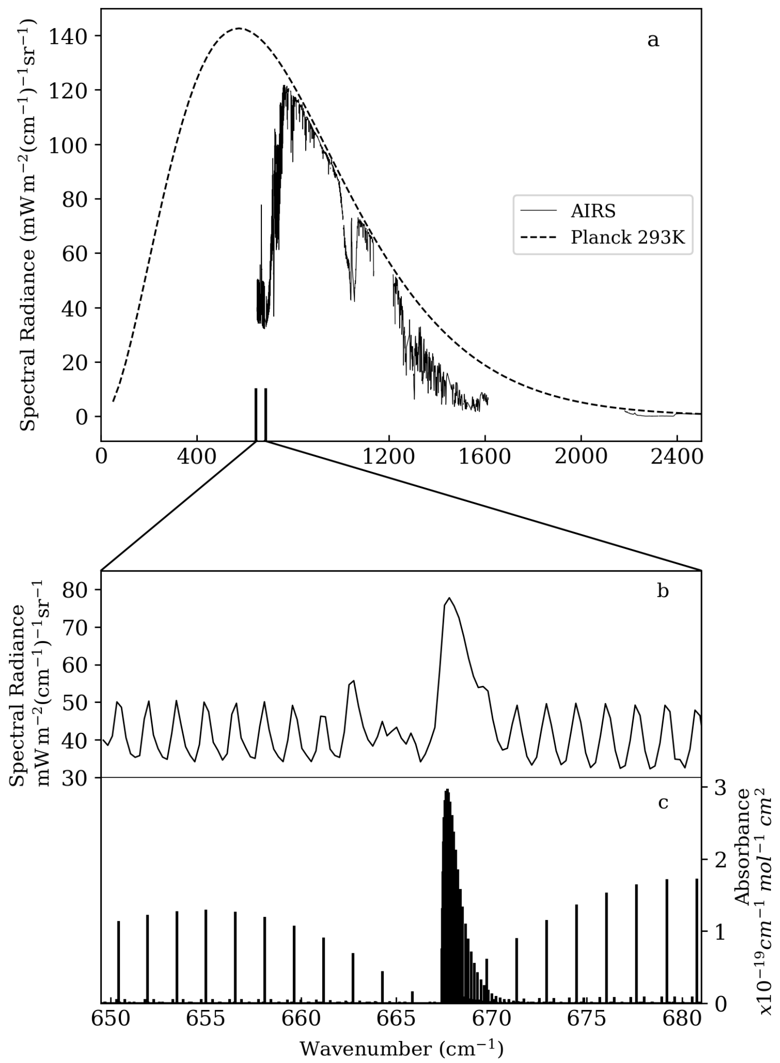

Figure 2. [a] AIRS nighttime, cloud-clear OLR spectrum and 293K Planck distribution, [b] 650-680 cm^{-1} subset, [c] HITRAN2016 spectral absorbance lines for CO_2 (Gordon et al., 2017). Note the excellent coincidence between AIRS detected radiance peaks and HITRAN CO_2 absorbance lines.

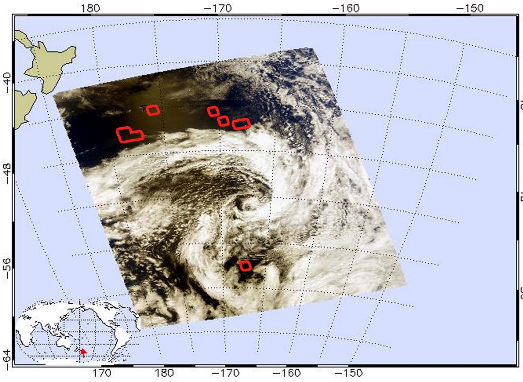

Figure 3. Visible image from granule 015 collected on January 1, 2016. Cloud-clear regions identified by the algorithm outlined in red.

meet this criterion. Although AIRS Level 2 measurements are a cloud-cleared data product, only naturally cloud-clear radiances with no mathematical adjustments contribute to this analysis. Figure 3 provides a cloud-clear selection example rendered from the sunlit side of Earth to permit comparison with a visible image, however no daytime OLR measurements contributed to this analysis. It is evident that the cloud detection algorithm is conservative: visibly cloud-clear areas were not included and no visibly cloud-contaminated areas were inadvertently included (in this example the cloud detection algorithm has false positives but no false negatives).

Solar longwave infrared radiation reflected by clouds or Earth's surface will combine with terrestrial OLR, contaminating daytime measurements. To eliminate this source of error, only nighttime measurements were utilized. When the AIRS solar zenith angle (SZA) is $<90°$ AIRS observes the sunlit side of Earth, when $90° < \text{SZA} < 108°$ it observes the twilight region and when $\text{SZA} \geq 108°$ it observes the nighttime region. Only measurements at $\text{SZA} \geq 108°$ were utilized.

The AIRS mirror scans $\pm 49.5°$ from nadir and higher scan angles observe IR emission from from higher in the atmosphere. Radiances from scan swath edges are significantly warmer or colder than nadir observations in the bands of radiatively-active gasses. To reduce the effects of this anisotropy, only radiances at scan angles $\leq 25°$ were utilized.

The 2,378 individual channels comprising the AIRS IR sensor are monitored for quality and flags are raised (0-2) whenever any should degrade. Measurements with quality value 0 "highest quality" and 1 "useful for scientific measurement" were utilized, while quality value 2 "do not use" were excluded. Radiance measurements flagged as dust-contaminated were similarly excluded, though these were rare ($<0.01\%$).

2 Method

All AIRS radiance measurements meeting the selection criteria were analyzed in this study (not a subset). Radiances for a given wavenumber channel were binned by month, sub-binned in 10° latitude increments, then averaged. For example, 4,554 nighttime, cloud-clear radiances at 650.814 cm^{-1} measured between 0° and 10°N contribute to the average radiance for January 2013 (figure 4, inset). 28.8% of sub-bins contain no data due to heavy clouds, lack of nighttime measurements (e.g., polar summers) or failed detector channels. An additional 1.2% of all sub-bins containing fewer than 25 radiances meeting the selection criteria were excluded to prevent trend skew by only a few measurements. The median number of radiance measurements contributing to a monthly average for a

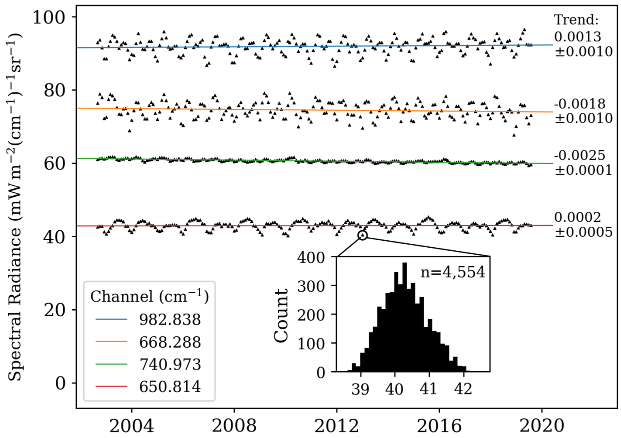

Figure 4. Least-squares regression fit to average monthly radiances for four AIRS channels in 0°-10° latitude bin. Remaining channels in all latitude bins were fit similarly.

given channel in a given latitude bin is 5,064. Over time, some channel detectors succumb to solar radiation exposure and cease useful data production. Of the maximum potential 17 year record, channels with fewer than five years were excluded for insufficient record length.

A straight line was fit by least-squares regression to the time series of monthly radiance averages for each channel in each latitude bin. Seasonal temperature cycling was eliminated as a source of trend bias by utilizing only complete years of measurement data starting on 1 September 2002 and ending on 31 August 2019. An example line fitting is provided in figure 4. The slope of each line is the spectral radiance trend $\dot{L}_{\tilde{\nu}}$ ($\mathrm{mW\,m^{-2}(cm^{-1})^{-1}sr^{-1}yr^{-1}}$) and the uncertainty is $\pm 1\sigma$. Lines were fit to all channels in all 18 latitude bins.

3 Results: CO_2 Radiative Forcing

Reductions in OLR at 650-756 cm^{-1} are presumed the result of rising atmospheric CO_2 concentration. The reductions at detectable portions of the CO_2 P, Q, and R-branches (650-682 cm^{-1}) are minor compared to 687-756 cm^{-1} where the majority of detectable OLR reduction coincides with one of the CO_2 wings. OLR flux density change δE (Wm^{-2}) was produced by integrating the spectral radiance trend $\dot{L}_{\tilde{\nu}}$ over the range of CO_2-affected wavenumbers, then multiplying by 17 years and by π sr, regarding the atmosphere as a Lambertian emitter at these optically-thick channels:

$$\delta E_{PQR} = 17\pi \int_{649.6cm^{-1}}^{682.0cm^{-1}} \dot{L}_{\tilde{\nu}} d\tilde{\nu} = -0.031 \pm 0.014\, Wm^{-2} \tag{1}$$

$$\delta E_{wing} = 17\pi \int_{687.6cm^{-1}}^{756.3cm^{-1}} \dot{L}_{\tilde{\nu}} d\tilde{\nu} = -0.164 \pm 0.033\, Wm^{-2} \tag{2}$$

Integrals are depicted in the figure 6 inset, shaded regions. The majority of detectable flux density change is attributable to the increasing wing absorption at 687-756 cm^{-1}. The symmetrical wing at 580-650 cm^{-1} is outside of AIRS measurement range (see figure 7). Consequently, (1) + (2) is only a partial measurement of δE caused by rising CO_2 and δE_{total} must be estimated. The P-branch and R-branch absorption lines flanking the Q-branch are nearly symmetrical and rising CO_2 caused nearly-identical reductions in radiance. By extension, it is a reasonable prediction that the unmeasured 580-650 cm^{-1} wing has undergone OLR reduction by an amount similar to the measured 687-

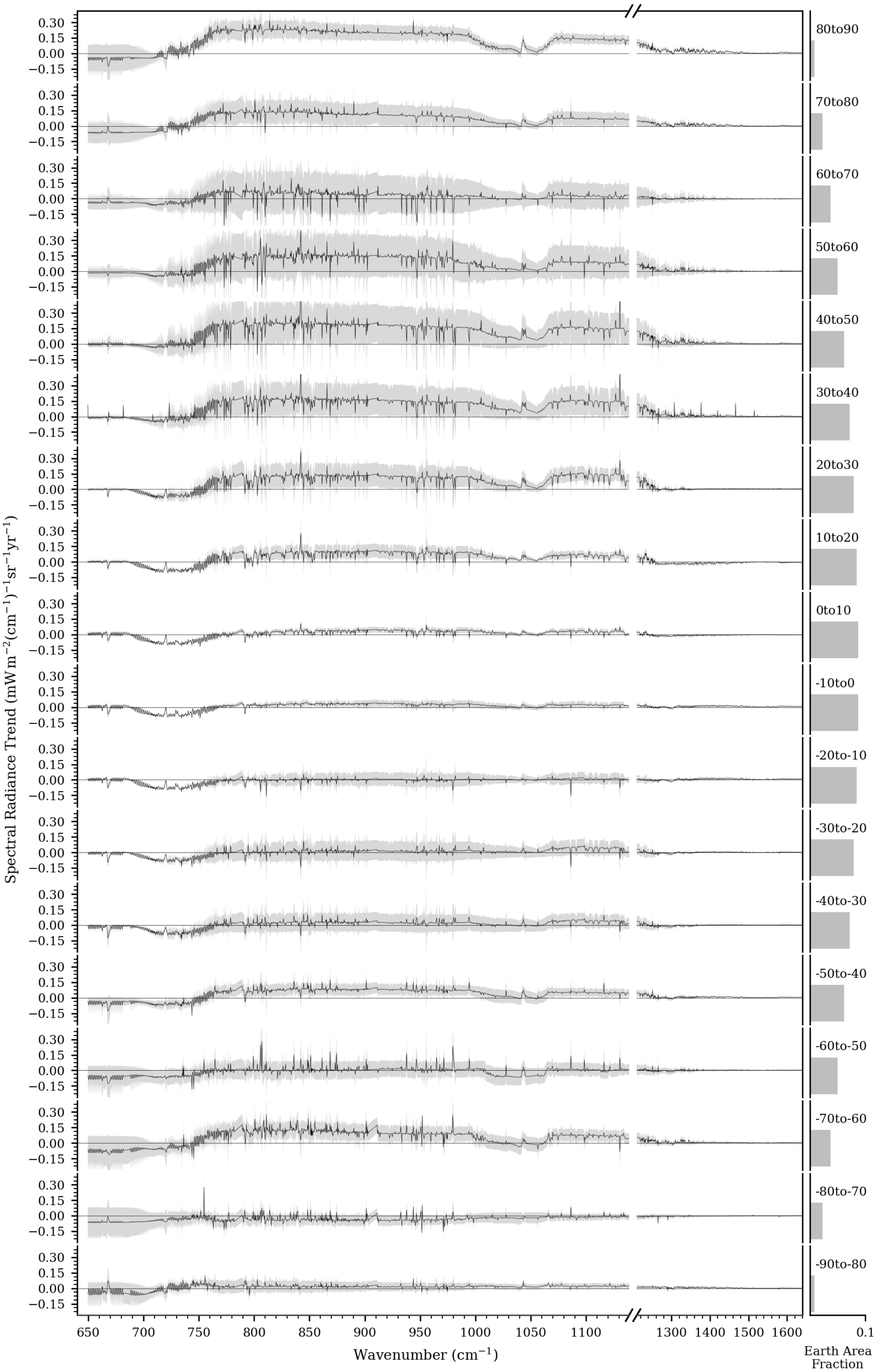

Figure 5. Nighttime, cloud-clear spectral radiance trend 2002-2019 in 10° latitude increments. $\pm 1\sigma$ shaded.

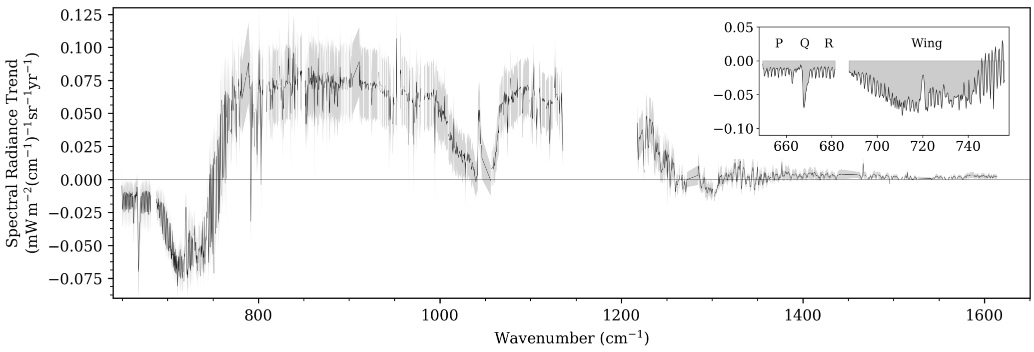

Figure 6. Global composite nighttime, cloud-clear spectral radiance trend 2002-2019. $\pm 1\sigma$ shaded. Inset illustrates the integrals assessed to determine OLR reduction attributable to rising CO_2.

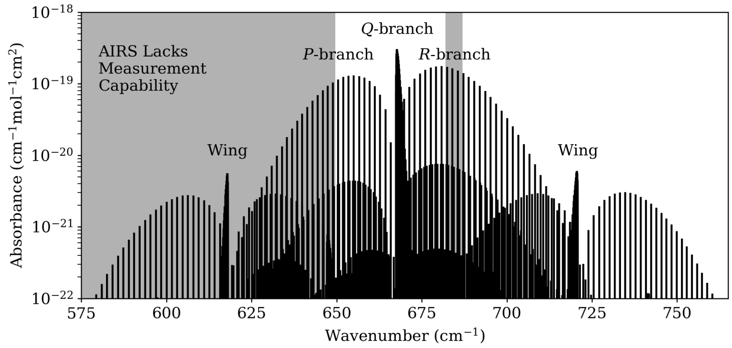

Figure 7. HITRAN2016 CO_2 v_2 absorption lines and AIRS measurement ranges

756 cm^{-1} wing. Therefore, total OLR flux density reduction due to rising CO_2 is estimated as:

$$\delta E_{total} = \delta E_{PQR} + 2\delta E_{wing} = -0.358 \pm 0.067\, Wm^{-2} \tag{3}$$

The computed flux density change, with reversed sign, is termed *radiative forcing* (RF). It is reasonable to view (1) + (2) as a partial global measurement of nighttime, cloud-clear CO_2 RF and (3) as an empirically-derived estimation of total nighttime, cloud-clear CO_2 RF added between 2002-2019.

Measurement of the atmospheric CO_2 concentration increase that produced this additional forcing was supplied by the NOAA ESRL's global monitoring division (Dlugokencky & Tans, 2019). The combination of empirical measurement of TOA RF and CO_2 concentration change permits a direct comparison to the climate model predictions of CO_2-induced effective radiative forcing (ERF) taken from the IPCC's Fifth Assessment Report (Stocker et al., 2013), also known as AR5. ERFs for 2000-2020 (368.9-412.1 ppm CO_2) were interpolated for 2002-2019 (373.1-410.5 ppm CO_2) and compared to AIRS measurements in table 1.

AR5 ERFs were computed while holding surface temperature constant, a condition that does not hold for Earth. Therefore, an additional comparison was sought to AIRS measurements of locations where surface/lower tropospheric temperatures did not significantly change. Window wavenumber trends in Figure 5 indicate this is largely true for 10°N-40°S and the area-weighted average forcing for this latitude range was included in table 1. In either case, AR5 climate models appear to over-predict CO_2 RF.

Table 1. Radiative Forcing from +37 ppm CO_2

Source	$-\delta E_{total} \pm 1\sigma$ (Wm^{-2})
AIRS 90°N-90°S	0.358±0.067
AIRS 10°N-40°S	0.434±0.047
IPCC AR5 ERF	0.508±0.102

4 Sources of Error

Radiance and flux density changes in the CO_2 v_3 band (2300-2380 cm^{-1}) were not characterized since less than 0.01% of the Earth's infrared radiant exitance occurs in this band.

The AIRS instrument measurement gap at 681.993-687.601 cm^{-1} prevents trend quantification in a narrow portion of the v_2 R-branch. Interpolation from adjacent channels yields 0.0038 Wm^{-2} of forcing was not measured, causing underestimate of δE_{total} by 1.2%.

The unmeasured 580-650 cm^{-1} wing was assumed to undergo radiance reduction identical to the measured wing, however, the 580-650 cm^{-1} wing overlaps with stronger water vapor absorption lines. The assumption of symmetry is conservatively high and actual OLR reductions at 580-650 cm^{-1} are expected to be lower than at 687-756 cm^{-1}. Trend asymmetry between the two wings was observed in DLR reported by Feldman et al. (2015): the 580-650 cm^{-1} wing showed less forcing change over time relative to the 687-756 cm^{-1} wing, particularly in the southern great plains where atmospheric moisture content is higher.

Over 17 years, detector stability is more important than absolute accuracy as unbiased noise does not preclude long-term trend analysis. One possible cause of trend bias is gradual accumulation of molecular contaminants on the AIRS detector mirror. A hypothetical 100Å contamination layer is predicted by H. Aumann et al. (2000) to increase the mirror emissivity variation by 0.001, producing cold scene brightness temperatures at 650-800 cm^{-1} that are 0.1-0.2° K warmer than reality. If such a contamination layer were gradually building up during the observation period, warming trends could be amplified and cooling trends (including forcing) could be diminished. Evidence of mirror contamination between 2002-2010 has been reported by others (H. H. Aumann et al., 2018) to affect AIRS midwave IR channels (2181-2665 cm^{-1}) which were not utilized in this study.

This analysis assumed isotropic atmospheric emissions despite radiances from scan swath edges measuring significantly warmer or colder than nadir observations. Over time, if proportionally more (or fewer) swath edge measurements meet the quality and cloud-clear selection criteria, trend bias will result. As a check, trend fits and integrals were recomputed with a wider and narrower scan angle ranges, including and excluding larger portions of scan swath edges. Fewer total measurements contribute to a restricted scan angle analysis with a commensurate increase in uncertainty. Results in table 2 indicate that including scan swath edges causes overestimation of forcing: δE_{total} produced from ±25° and ±49.5° measurements are 3.8% and 10.4% higher than from ±12.5° measurements, respectively.

Table 2. Swath Edge Radiance Impact

Scan Angle	Radiances at 650-756 cm^{-1}(count)	CO_2 Forcing $-\delta E_{total} \pm 1\sigma(\text{Wm}^{-2})$
±49.5°	$25.7\text{x}10^9$	0.381±0.067
±25.0°	$15.5\text{x}10^9$	0.358±0.067
±12.5°	$7.8\text{x}10^9$	0.345±0.068

5 Conclusion

Seventeen years of AIRS nighttime, cloud-clear OLR measurements reveal 0.358±0.067 Wm^{-2} additional radiative forcing induced by +37 ppm atmospheric CO_2. Unfortunately, AIRS lacks measurement capability at 580-650 cm^{-1} for complete CO_2 v_2 band characterization, therefore this empirical estimate of increased forcing was devised by presuming CO_2 v_2 wing symmetry and doubling the observed wing's radiative forcing. The IPCC Fifth Assessment Report predicted 0.508±0.102 Wm^{-2} RF resulting from this CO_2 increase, 42% more forcing than actually observed. The lack of quantitative long-term global OLR studies may be permitting inaccuracies to persist in general circulation model forecasts of the effects of rising CO_2 or other greenhouse gasses.

Acknowledgments

The author acknowledges Robert Amour and Leon de Almeida for analysis program creation, Nolan Nicholson for the custom data plotting program and Steven J. Martin for the many informative conversations. All code for analysis replication is available at `https://github.com/rentcp/Heatwave`.

References

Aumann, H., Gregorich, D., Gaiser, S., Hagan, D., Pagano, T., Strow, L., & Ting, D. (2000). Airs algorithm theoretical basis document. *Level 1B, Part*, *1*, 70.

Aumann, H. H., Manning, E. M., & Broberg, S. (2018). Radiometric stability in 16 years of airs hyperspectral infrared data. In (Vol. 10764, p. 107640O).

Dlugokencky, E., & Tans, P. (2019). *Noaa/esrl.* `www.esrl.noaa.gov/gmd/ccgg/trends/`. (Accessed 11-2019)

Feldman, D. R., Collins, W. D., Gero, P. J., Torn, M. S., Mlawer, E. J., & Shippert, T. R. (2015). Observational determination of surface radiative forcing by co2 from 2000 to 2010. *Nature*, *519*(7543), 339.

Gordon, I. E., Rothman, L. S., Hill, C., Kochanov, R. V., Tan, Y., Bernath, P. F., ... others (2017). The hitran2016 molecular spectroscopic database. *Journal of Quantitative Spectroscopy and Radiative Transfer*, *203*, 3–69.

Harries, J. E., Brindley, H. E., Sagoo, P. J., & Bantges, R. J. (2001). Increases in greenhouse forcing inferred from the outgoing longwave radiation spectra of the earth in 1970 and 1997. *Nature*, *410*(6826), 355.

Stocker, T. F., Qin, D., Plattner, G.-K., Tignor, M., Allen, S. K., Boschung, J., ... others (2013). Climate change 2013: The physical science basis.

Teixeira, A. S. T. (2013). *Airs/aqua l2 cloud-cleared infrared radiances (airs-only) v006.* `https://doi.org/10.5067/Aqua/AIRS/DATA205`. (Accessed 10-2019)